Predicting adsorption behavior and anti-inflammatory activity of naproxen interacting with pure boron nitride and boron phosphide fullerene-like cages

Yan Cao [a], Afrasyab Khan [b], Fatemeh Ghorbani [c], Hassan Mirzaei [d], Preeti Singla [c], Hanzaleh Balakheyli [c], Alireza Soltani [c,e,*], Mehrdad Aghaei [c,**], Zivar Azmoodeh [c], Mehdi Aarabi [c], Samaneh Tavassoli [c]

[a] School of Mechatronic Engineering, Xi'an Technological University, Xi'an 710021, China
[b] Institute of Engineering and Technology, Department of Hydraulics and Hydraulic and Pneumatic Systems, South Ural State University, Lenin Prospect 76, Chelyabinsk 454080, Russian Federation
[c] Golestan Rheumatology Research Center, Golestan University of Medical Science, Gorgan, Iran
[d] Ischemic Disorders Research Center, Golestan University of Medical Sciences, Gorgan, Iran
[e] Cancer Research Center, Golestan University of Medical Sciences, Gorgan, Iran

ARTICLE INFO

ABSTRACT

The adsorption of naproxen (NPX) on surface of the boron phosphide (BP) and boron nitride (BN) fullerene-like cages have been studied and discussed by using density functional theory (DFT) and time-dependent density functional theory (TDDFT) calculations. Adsorption results using DFT demonstrated that $B_{12}N_{12}$ have strong interactions with the carbonyl (-C = O) group of naproxen via covalent bonding, while the interaction of the naproxen through a carbonyl and hydroxyl groups with the $B_{12}P_{12}$ occurred via electrostatic interactions, suggesting a large desorption time due to a large negative adsorption energy. The effects of hydroxyl (OH) functionalization on the adsorption of NPX via $B_{12}N_{12}$ has also been investigated. Results reveal that OH functionalization decreases the absolute E_b value of NPX on studied $B_{12}N_{12}$ fullerene-like cage. Theoretical studies also demonstrated the frequency shifts that is happening because of the adsorption process. The electronic and optical properties of $B_{12}N_{12}$ and OH-$B_{12}N_{12}$ in the presence of NPX are significantly sensitive. Interaction results demonstrated that $B_{12}N_{12}$ with H-donor functional groups such as –OH was effective for the delivery of naproxen as it leads to an increased dipole moment with weak binding energy. The polarity for the NPX loaded OH-$B_{12}N_{12}$ shows the feasibility of ameliorating the situation of solubility desirable for drug delivery systems in biological devices. Through the analysis of molecular docking, it was found that NPX loaded OH-$B_{12}N_{12}$ is potent inhibitors of TNF-α receptor and IL-1 receptor targets compared to $B_{12}N_{12}$ and $B_{12}P_{12}$ systems.

© 2021 Elsevier B.V. All rights reserved.

1. Introduction

Naproxen [6-methoxy-α-methyl-2-naphthalene acetic acid] is one of the most widely prescribed non-steroidal anti-inflammatory drugs (NSAIDs) especially for in the case of different type of musculoskeletal disorders like arthritis and low back pain owing to its desirable anti-inflammatory, analgesic, and antipyretic features. Generally, NSAIDs works great in the musculoskeletal dis-eases as anti-inflammatory agents by blocking cyclooxygenases (COX-2) in the central nervous system [1–3]. Due to poor aqueous solubility and permeability, NPX represents low absorption and poor bioavailability which restrict its treatment efficacy. Accordingly, using novel drug delivery systems may ameliorate bioavailability and therewith improve NPX pharmacokinetics [2]. Boron nitride (BN) nanomaterials owing to their unique chemical and physical features have been emerged as an efficient nanocarrier in the field of nanomedicine that can revolutionize the drug delivery systems [4]. In this study, the adsorption behavior of NPX has been extensively examined over the surface of $B_{12}N_{12}$ and $B_{12}P_{12}$ fullerene-like cages, in addition the anti-inflammatory activity of NPX has also been evaluated before and after the adsorpiton.

The discovery of the boron nitride (BN) fullerenes such as $B_{12}N_{12}$, $B_{24}N_{24}$, $B_{36}N_{36}$, and $B_{60}N_{60}$ shortly after the success of carbon fullerenes, play a vital role for the introduction of nanotechnology in the biomedical field. Owing to remarkable properties of BN nanostructures including constant band gap i.e. 6 eV, high-temperature stability, low dielectric constant, large thermal conductivity and high oxidation resistance, they successfully supersede their carbon counterparts in most of the applications such as in environmental purification, biomedical treatment, and sensing properties [5–16]. High surface to volume ratio of fullerene among all other nanostructures reinforced them as an ideal candidate in the field of adsorption. Among numerous $(BN)_n$ clusters (n = 4–30), the smallest cluster that was theoretically foreseen and satisfies isolated tetragonal laws is $B_{12}N_{12}$. Moreover, shortly afterwards $B_{12}N_{12}$ fullerene was successfully synthesized by laser desorption time-of-flight mass spectrometry [17–19]. Structurally, $B_{12}N_{12}$ fullerene consists 4 and 6 membered rings of alternatively bonded boron and nitrogen atoms [20,21]. Due to high biocompatibility and non-cytotoxicity of BN nanostructures, they have attracted wide attention of the researchers in the biomedical field to be used as nano-carriers for drugs [22,23]. In one study, the amino group grafted of mesoporous silica (MS)-functionalized boron nitride nanospheres exhibited no cytotoxicity and enhanced the delivery of CpG oligodeoxynucleotides into macrophages [24]. Recently, many computational predictions have been reported on the applications of BN nanocages like removal of organic pollutant molecules [25–27], biosensor [28,29], and drug delivery systems [30,31]. Furthermore, desired solubility/suspensibility of BN nanostructures can also be attained by their surface modifications such as functionalization with hydroxyl groups (OH) [32,33], alkyl chains [34], and wrapping by polymer molecules [35–41]. For instance, Weng et al. [42] have reported that high hydroxylation of BN nanomaterial's made them porous, nontoxic, stable and soluble in physiological solutions and hence was used for anticancer drug delivery by carrying doxorubicin on their surface. Weng et al. demonstrated that h-BN porous sheets with richly exposed (002) plane edges terminated by hydroxyl (—OH) groups can lead to redshifts in its absorption spectrum and function as a visible light sensitizer [43]. Recently, Grant et al. also pointed out which (002) planes with O-terminated edge site of h-BN function as active sites for selective oxidative dehydrogenation of propane to propene [44]. Farmanzadeh and Keyhanian have theoretically indicated that the amantadine adsorption upon the surface of $B_{12}N_{12}$ fullerene was exothermic with release of about −44.42 kcal/mol in gas phase and −50.68 kcal/mol in water phase [45]. Furthermore, In a DFT study, $B_{12}N_{12}$ can be used as a nanocarrier for both the 5-fluorouracil (5-FU) drug and its tautomeric forms by forming strong (covalent bond) interactions and week interactions respectively [46]. Adsorption behavior of metformin drug on pure and doped boron nitride fullerenes has also been studied in both air and water environments [47] in which results revealed that the NH group of metformin can chemically adsorbed upon the boron atom of $B_{12}N_{12}$ and $B_{16}N_{16}$ fullerenes. Cairo *et al.* reported the effect of NPX on the serum levels of IL-I, IL-6 and TNF-alpha in 18 patients with osteoarthritis. They found that the patients receiving treatment with NPX had a statistically remarkable decrement of the serum levels of IL-1b and IL-6 [48]. Guilherme et al. presented that nanostructured lipid carrier (NLC) loaded with NPX as a promising candidate for the safe treatment of inflammatory pain conditions of the temporomandibular joint or other joints. They found that the NLC-NPX formulation for the inflammatory conditions of the temporomandibular joint remarkably decreased leukocytes migration and levels of IL-1β and TNF-α [49].

Herein, we have studied the adsorption behavior and anti-inflammatory activity of NPX on the outer surfaces of $B_{12}N_{12}$ and $B_{12}P_{12}$ fullerene-like cages as drug delivery vehicles. Simulated IR

and UV–visible spectra of the NPX-$B_{12}N_{12}$ and NPX-$B_{12}P_{12}$ systems (DFT level) has been computed and compared with the experimental data. Furthermore, in the hybrid M06-2XD functional, double Hartree-Fock exchange has also been included to improve the description of non-covalent interactions.

2. Methodology and computational details

The geometries of the $B_{12}N_{12}$, $B_{12}P_{12}$, NPX and their adsorbed systems in various orientations have been fully optimized and evaluated by the M06-2X-D (dispersion-corrected *meta*-GGA hybrid) functional and 6-311G** basis set as this is most appropriate basis set for inorganic nanomaterials [50–52]. The M06-2X introduced as a global hybrid functional with 54% HF exchange that is appropriate for uses at the nanoscale molecular systems. Moreover, good reliability of M06-2X hybrid density functional has formerly been shown in calculating molecular binding energies of different drugs on the $B_{12}N_{12}$ fullerene-like cage [53,54]. In order to mimic the biological system, effect of solvent (water) has also been taken into account by using the PCM (polarizable continuum model) [55]. We have also investigated frontier molecular orbital (FMO), total density of states (TDOS), molecular electrostatic potential (MEP), and Mulliken population analysis (MPA) to determine other substantial parameters of the various interacting systems. M06-2X-D functional has been performed for more accuracy by DFT formalism implemented in Gaussian 09 package [56]. Basis set superposition error (BSSE) for the binding energy was determined using counter poise correction method. TDDFT (time-dependent density functional theory) calculations and thermodynamic parameters have also been carried out by incorporating the M06-2X/6-311G** level of theory. Furthermore, the M06-2X functional has also been discussed to obtain high precision in adsorption energy values. The adsorption energy (E_b) of NPX over the surface of BN fullerene is defined by:

$$E_b = E_{Fullerene-NPX} - (E_{Fullerene} + E_{NPX}) + E_{BSSE} \qquad (1)$$

where $E_{Fullerene}$, E_{NPX} and $E_{Fullerene-NPX}$ are the total energy of the pristine $B_{12}N_{12}$ fullerene-like cage, NPX molecule and NPX adsorbed $B_{12}N_{12}$ complex respectively. Molecular docking calculations was achieved using Auto Dock software (4.2) [57]. The crystal structures of tumour necrosis factor alpha (TNF alpha) (PDB ID: 2AZ5) and interleukin (IL)-1A-S100A13 complex (PDB ID: 2L5X) was provided from protein data bank. The crystal structure of the proteins was constructed using a process where the cognate ligand was, eliminated, hydrogen atoms and non-polar hydrogens were determined by Auto Dock Tools (ADT). We design a Lamarckian genetic algorithm for local search method and used grid map of 60×60×60 with 0.375 Å grid spacing for preparation of autogrid [58,59].

3. Results and discussion

3.1. Structural analysis of NPX and $B_{12}N_{12}$

The structural parameters of NPX drug and $B_{12}N_{12}$ fullerene-like cage have been measured from their fully optimized geometries using M06-2X functional in Figs. 1 and 2 respectively. The accuracy of M06-2X functional has been administrated by comparing the obtained data with the already reported literature values (Table S1). Furthermore, molecular electrostatic potential (MEP), infrared (IR) spectrum, the highest occupied molecular orbital (HOMO), and the lowest unoccupied molecular orbital (LUMO) of the NPX and $B_{12}N_{12}$ fullerene have also been presented alongwith optimized geometries in Figs. 1 and 2 repsectively.

The electron densities in the HOMO and LUMO maps of NPX have been observed to be more constrained over C atoms of the
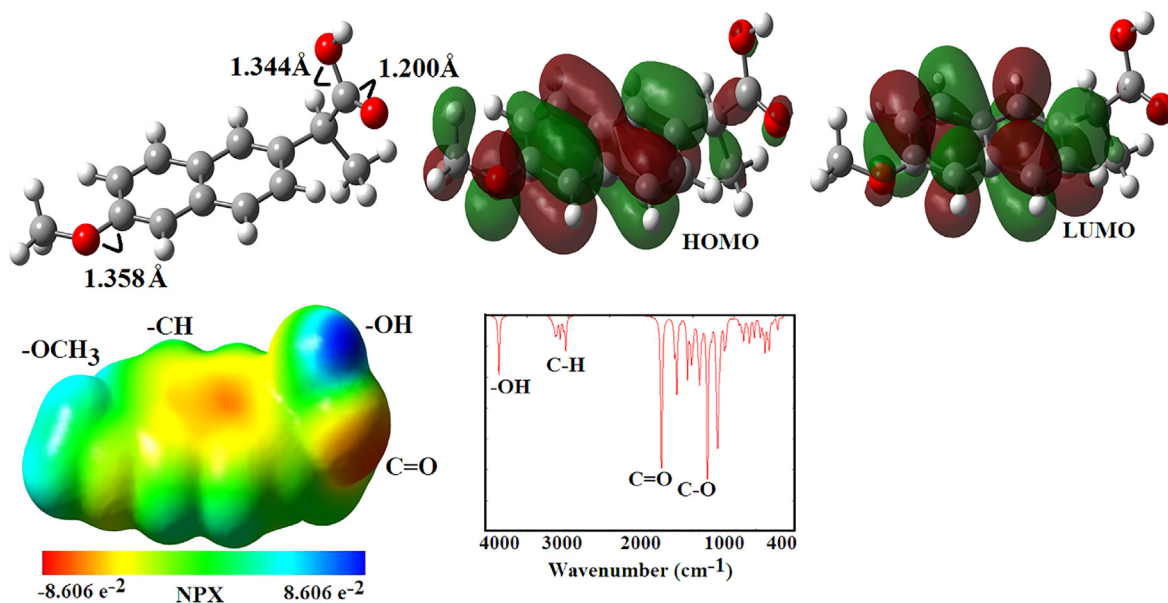
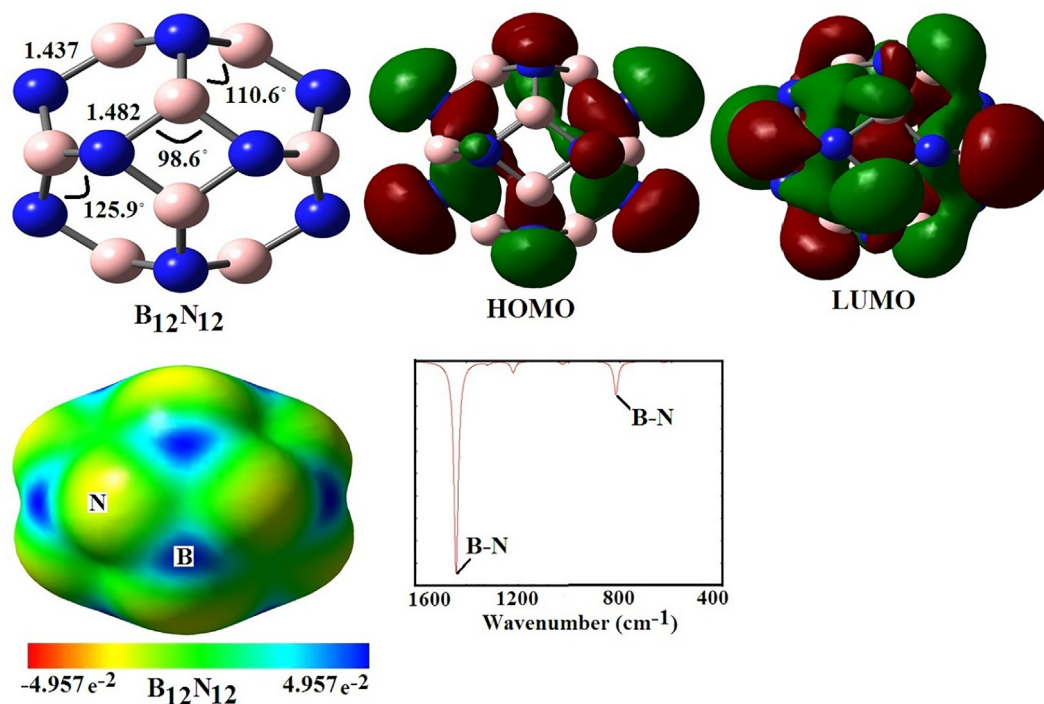**Fig. 1.** Optimized structure, MEP plot, IR spectrum and HOMO and LUMO profiles of NPX drug molecule.

Fig. 2. Optimized configuration, HOMO and LUMO profiles, MEP plot and IR spectrum of $B_{12}N_{12}$ fullerene-like cage.

naphthalene ring as compared to that of bonded to highly electronegative O atoms. The electrostatic potential scan of NPX have visually distinguished the oxygen atom of carbonyl group (—C=O) as negative potential surface with red color that acts as a nucleophilic site. Moreover, the IR spectrum of NPX in the range of 4000–400 cm^{-1} has clearly indicated the O—H and C=O stretching vibrations at 3342 cm^{-1} and 1728 cm^{-1} respectively, which was found to be in concordance with the experimental data [60].

The optimized structure of $B_{12}N_{12}$ fullerene (Fig. 2) has demonstrated a hollow cluster of four- and six-membered rings having an average B-N bond length of 1.482 and 1.437 Å respectively [61,62]. HOMO is found to be mainly localized over the N atom while

LUMO is distributed over the B atoms. Moreover, the polar nature of B-N bond has also been reflected from the MEP plots showing positive potential over B (blue color) and negative on the N (yellow color) atoms. IR spectrum has indicated the characterstic peaks of B-N bonds at 816 and 1440 cm^{-1}.

3.2. Adsorption of NPX on $B_{12}N_{12}$ fullerene

With the aim to account most interactive site of NPX, different orientations considering all possible sites of interactions between NPX and $B_{12}N_{12}$ fullerene-like cage have been optmized (Fig. 3). State I has represented the interaction through carbonyl group,
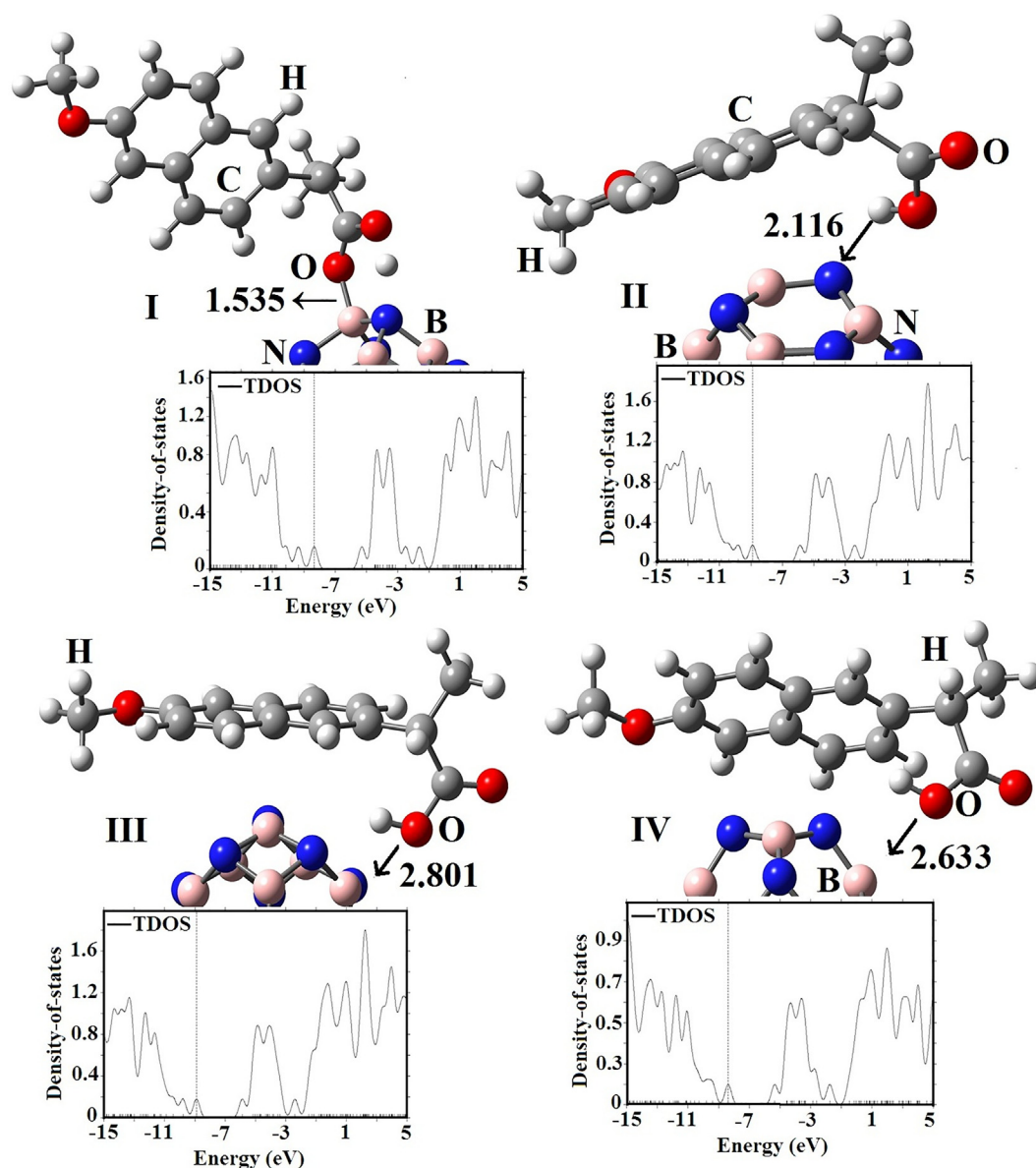
Fig. 3. Optimized configuration and TDOS plot for NPX-$B_{12}N_{12}$ complex in different orientations (I) state I, (II) state II, (III) state III and (IV) state IV.

state II has shown the interaction of H atom of hydroxyl group with N atom of $B_{12}N_{12}$ fullerene, states III and IV have accounted the interactions between O atom of hydroxyl group with the $B_{12}N_{12}$ fullerene-like cage. By analysing the adsorption energy (E_{ad}) i.e. energy change during the adsorption of NPX molecule over the surface of $B_{12}N_{12}$ fullerene-like cage in different orientations, it has been observed that state I is the most stable orientation with the release of maximum energy i.e. −29.75 kcal/mol as compared to state II, III and IV with corresponding values of −8.99, −21.45, −9.68 kcal/mol respectively. However, the adsorption process is highly feasible in every state indicated by the negative value of E_{ad}. Kian and Tazikeh-Lemeski reported that the aromasin via carbonyl group can be chemically adsorbed on $B_{12}N_{12}$ fullerene-like cage with a energy of −23.05 kcal/mol [63]. In a similar study, the carbonyl group of 5-aminosalicylic acid (−24.89 kcal/mol), as a non-steroid anti-inflammatory drug, plays a significant role on the adsorption energy with the boron atom of $B_{12}N_{12}$ fullerene-like cage in comparison to the amino (−21.20 kcal/mol) and hydroxyl (−19.13 kcal/mol) groups [64]. Furthermore, to scrutinize the insights of nature of interactions between NPX and $B_{12}N_{12}$

fullerene-like cage in all states, nearest-neighbour distance (summarized in Table 1) has been estimated and found to be 1.535 Å, 2.116 Å, 2.634 Å and 2.633 Å for state I, II, III and IV respectively. The large distance in the state II, III and IV has inferred the presence of long-distance interactions i.e. through weak van der Waals forces [65].

However, the short distance in state I has elucidated the existence of covalent bond between electron rich O atom of —C=O group of NPX and electron deficient B atom of the $B_{12}N_{12}$ fullerene-like cage. In contrast to the physisorption, presence of chemisorption in state I has further been ensured by analyzing other important parameters. Significant charge transfer i.e. 0.21e (calculated using Mulliken charge analysis) from NPX to $B_{12}N_{12}$ fullerene-like cage has favored the chemical nature of interactions in state I. Moreover, increment in the B-N bond length i.e. from 1.437 Å to 1.562 Å and 1.482 Å to 1.549 Å after adsorption in four- and six membered rings respectivley put an another evidence in favour of chemisorption in state I. To assess the spontanity and change in enthalpy during the adsorption process, thermodynamical parameters including Gibbs free energy change (ΔG) and the

Table 1
Values of adsorption energy, nearest-neighbor distance, thermodynamic parameters and dipole moment of all the states in the gas phase.

State	E_{ad}/kcal/mol	D/Å	ΔG/kcal/mol	ΔH/kcal/mol	μ_D/Debye
I	−29.75	1.535	−4.84	−8.53	7.59
II	−8.99	2.116	4.61	−7.63	6.32
III	−21.45	2.634	−3.69	−9.68	8.12
IV	−9.68	2.633	5.30	−8.99	6.08
G	−14.53	2.597	0.19	−12.09	4.49
H	−0.92	3.074	3.88	−8.17	5.84
OHB$_{12}$N$_{12}$	−60.19	1.342	−40.76	−30.37	1.62
X	−15.91	1.518	−18.81	−32.92	7.10
Y	−10.84	1.882	−19.55	−33.52	3.31

enthalpy change (ΔH) have also been estimated (summarized in Table 1). The negative value of ΔG and ΔH i.e. −4.84 and −8.53 kcal/mol respectively (for state I) clearly depicted the spontanity and exothermic nature of the adsorption process. The reduction in the amount of ΔG compared to ΔH can be explained by considering the entropic effect [66].

3.3. Role of N atom of B$_{12}$N$_{12}$ fullerene-like cage in the strength of interactions

As per the above discussion, it can be declared that state I i.e. the interaction of O atom of carbonyl group of NPX with B atom of B$_{12}$N$_{12}$ fullerene-like cage is very strong and leads to highly
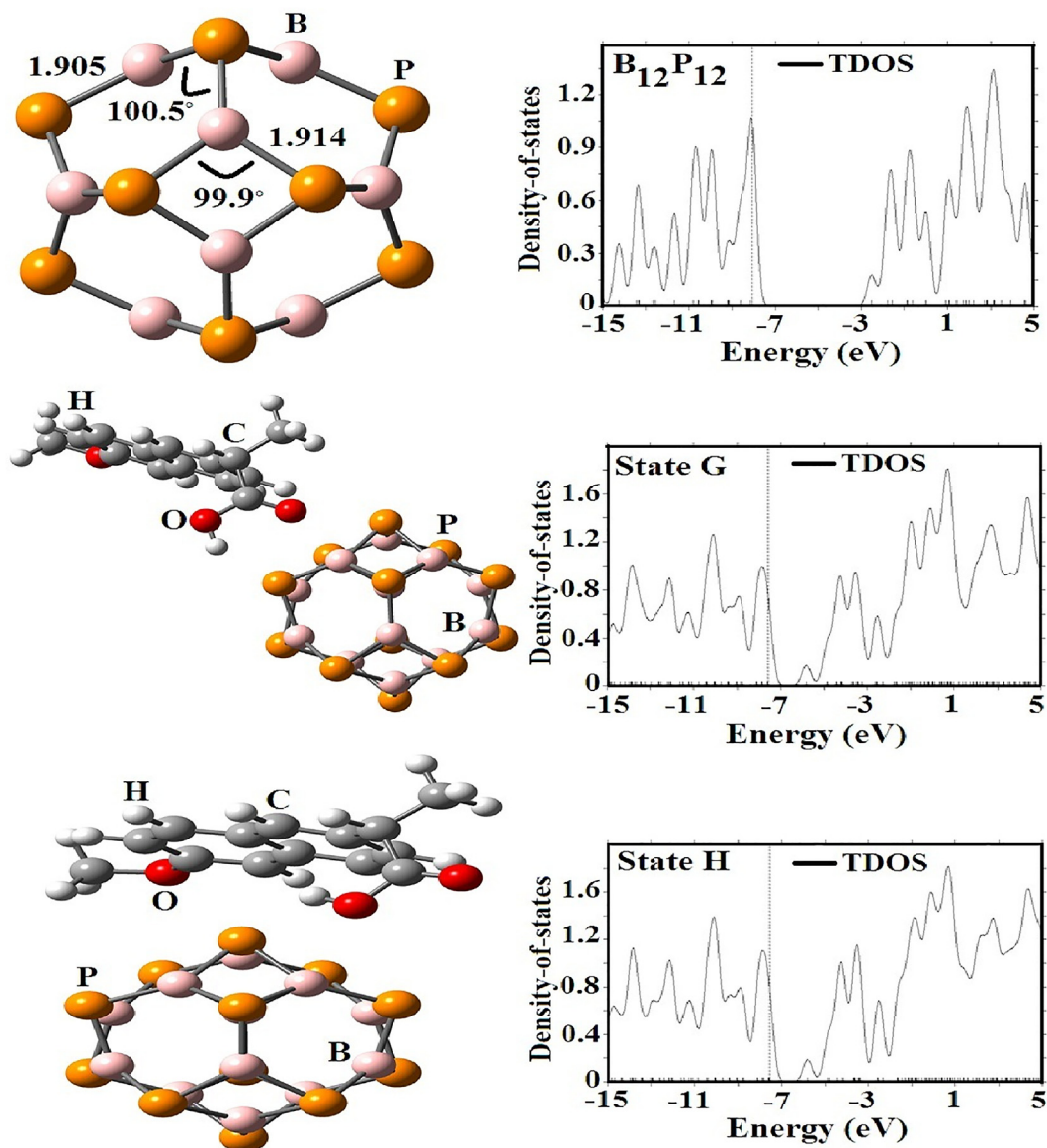

Fig. 4. Optimized configurations and TDOS plots of pristine B$_{12}$P$_{12}$ and different orientations of NPX adsorbed B$_{12}$P$_{12}$ fullerene-like cage.

stable covalently bonded complex. Major credit of these strong interactions goes to the N atom of the $B_{12}N_{12}$ fullerene that can be proved by replacing the N atom with the phosphorous (P) atom i.e. by studying the adsorption behaviour of NPX molecule over the surface of $B_{12}P_{12}$ fullerene-like cage. Two orientations i.e. interaction through —C=O (state G) and —OH (state H) (shown in Fig. 4) have been studied by employing same level of theory. The nature and strength of the interactions have been assessed on the basis of E_{ad} i.e. −14.53 kcal/mol and −0.92 kcal/mol and nearest-neighbour distance i.e. 2.597 Å and 3.074 Å for state G and H respectively. Low value of adsorption energy has illustrated the less stability of the NPX/$B_{12}P_{12}$ complex as compared to that of over the surface of $B_{12}N_{12}$ complex. Moreover, there is just 0.10e charge transfer from NPX to $B_{12}P_{12}$ fullerene-like cage which can be explained on the basis of low electronegativity of P that impose less electron withdrawing effect on the B atom and hence leads to generate weak electrostatic interactions. Thus it can be declared

that N atoms in $B_{12}N_{12}$ fullerene-like cage plays a key role to generate the significant electron deficient site i.e. at B atom to interact strongly with the nucleophilic sites of the adsorbate molecules. Similar results has also been reported by Rad and Ayub that adsorpiton of guanine is more stable over the surface of $B_{12}N_{12}$ as compared to $B_{12}P_{12}$ fullerene-like cage [67,68].

3.4. Adsorption of NPX on hydroxylated-$B_{12}N_{12}$ fullerene

In order to invigilate the effect of functionalization on the adsorption behaviour of NPX, $B_{12}N_{12}$ fullerene-like cage has been subjected to hydroxylation i.e. chemical functionalization of B atom by the hydroxyl group (—OH). Structural deformations including increment in the B-N bond length i.e. from 1.483 Å to 1.499 Å, N-B-N bond angle i.e. from 98.58° to 116.73° and increase in the dipole moment (μ_D) i.e. from 0 to 1.62 Debye has been explained by the transformation of hybridization of B atom from
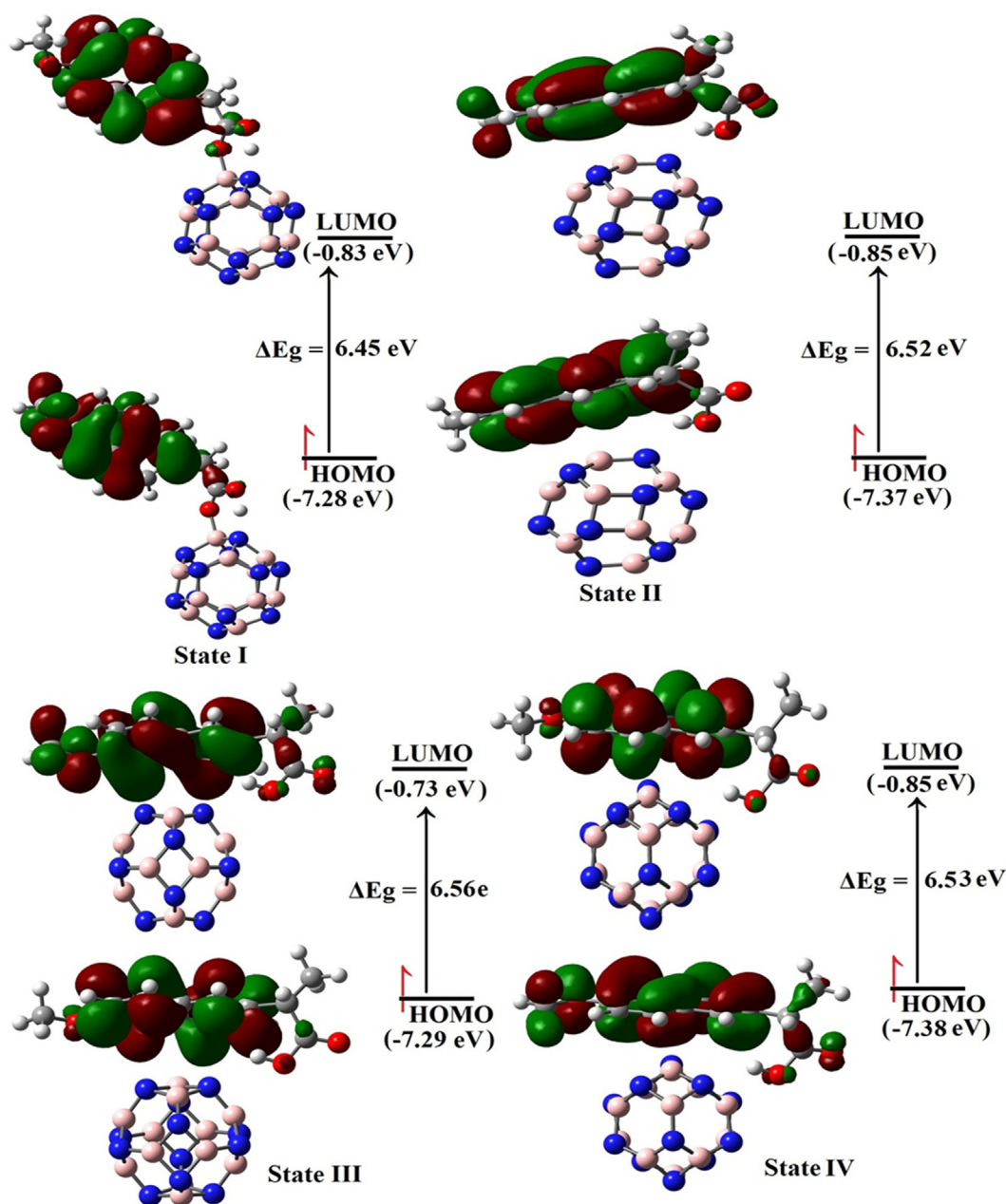

Fig. 5. HOMO-LUMO profiles of NPX-$B_{12}N_{12}$ complex in state I, II, III and IV.

sp^2 to sp^3 after hydroxylation [33,69–71]. The presence of hydroxyl group have enhanced the electrophilicity of B atom by withdrawing electron through more electronegative O atom. Afterwards, NPX drug molecule has been adsorbed over the surface of OH-$B_{12}N_{12}$ fullerene-like cage through two interactive sites i.e. carbonyl (state X) and hydroxyl (state Y) group. The optimized geometries of state X and Y are shown in Fig. 5. On the basis of the adsorption energy and nearest-neighbor distance i.e. −15.91 kcal/mol and 1.518 Å (state X) and −10.84 kcal/mol and 1.882 Å (state Y) respectively (Table 1), it can be deduced that the adsorption of NPX is more favourable through carbonyl group that is in concordence with the earlier results [11,21]. Analysis of the adsorption energy of state X (−35.53 kcal/mol) and Y (−39.61 cal/mol) reveals that M06-2XD functional does differ too much from M06-2X functional. This causes the M06-2XD functional more apprperiate a priori for the calculation in these adsorption systems. Furthermore, the presence of the covalent bonding between the NPX and OH-$B_{12}N_{12}$ fullerene-like cage in state X has been explained on the basis of short nearest-neighbor distance and large charge transfer (0.32e) from the NPX to OH-$B_{12}N_{12}$. As introduction of the polar hydroxyl group has remarkably polarized the $B_{12}N_{12}$ fullerene-like cage [72], hence makes them highly soluble in polar solvents (water). The solvation energy (E_{solv}) of the complex before and after the adsorption of NPX has been calculated i.e −2.58 and −0.57 eV respectively suggesting less solubilty of state X than the pure OH-$B_{12}N_{12}$ fullerene-like cage in water [16]. The small distance in the state X, although give rise to lower adsorption energies, but causes larger μ_D in the water phase because of great vector. The results from this study indicated that adsorption of NPX drug upon OH-$B_{12}N_{12}$ fullerene-like cage raises the polarity of the all system which is especially important for a vast variety of fullerene-like cage applications as nanovehicles for drug delivery [73–75].

3.5. Effect of solvent

To imitate the biological system, all the geometries have been subjected for reoptimization by PCM model with water as a solvent using same level of theory (M06-2X) [76]. The values of adsorption energy, nearest-neighbor distance and solvation energy of all the state are summarized in Table 2. The measured solvation energy (E_{solv}) of NPX on the $B_{12}N_{12}$ surface (state I) was −17.18 kcal/mol higher than that of the $B_{12}N_{12}$ fullerene-like cage (state G), as summarized in Table 2. The addition of a hydroxyl group on the $B_{12}N_{12}$ surface for interacting with NPX in water environment reduced E_{solv} by less than −15.45 kcal/mol relative to that for the pure $B_{12}N_{12}$ fullerene-like cage. In addition, the calculated E_{solv} for NPX on OH-$B_{12}N_{12}$ surface in dichloromethane environment was slightly more remarkable (with the values of −13.02 and −13.35 kcal/mol in states X and Y respectively) than that of the

$B_{12}N_{12}$ surface for interacting with NPX in water environment. On comparing these values, it has been observed that adsorption of NPX over the surface of $B_{12}N_{12}$ fullerene-like cage is slightly more stable in dichloromethane environment in comparison with water environment. These values present that OH-$B_{12}N_{12}$ surfaces are more soluble in water environment than the pure nanocages. These results augment the fact that NPX get physically adsorbed on the OH-$B_{12}N_{12}$ surface and this works in favour of the suitability of the fullerene-like cages considered here as nanocarrier in addition the drug release can be easily achieved by the desorption process [77].

3.6. Electronic properties

As summarized in Table 3 and by TDOS plots in Fig. 4, the electronic properties of $B_{12}N_{12}$ and OH-$B_{12}N_{12}$ fullerene-like cages are remarkably affected by the NPX adsorption. The HOMO and LUMO energies of the $B_{12}N_{12}$ and OH-$B_{12}N_{12}$ fullerene-like cages are altered on the NPX adsorption (see Figs. 5 and 6). The E_g values for the $B_{12}N_{12}$ and OH-$B_{12}N_{12}$ fullerene-like cages are calculated to 9.51 and 9.21 eV by M06-2X functional respectively, which is different with obtained results by B3LYP [78,79] and PBE methods [80,81]. The E_g value after NPX adsorption through the C=O group (state I) reduced about 32.17% in the gas phase and 32.07% in the water phase. In contrast with the pure fullerene, we observed that the adsorption of NPX on the fullerene-like cage in the presence of hydroxyl group have no distinct changes in the E_g values, this result was in accordance with the theoretical results obtained for the hydroxylation of a metal-supported hexagonal boron nitride monolayer [82]. As thses changes in the states X and Y are 29.75 and 29.85% in the gas phase and 30.37 and 30.16% in the water phase, respectively (see Table 4). Therefore, the change of E_g (ΔE_g) is noticible and the resistivity of conductivity of the fullerene will change remarkably [83]. The populations of conduction electrons of the $B_{12}N_{12}$ and OH-$B_{12}N_{12}$ fullerene-like cages at a given temperature (293.15 Kelvin) considerably altered by the adsorption of NPX hydrides owing to significant ΔE_g. Consequently, the presence of the NPX can be detected by the pure $B_{12}N_{12}$ and OH-$B_{12}N_{12}$ fullerene-like cages via the creation of noise [84].

The calculated molecular electrostatic potential (MEP) maps demonstrate that the strong positive electrostatic potential happen upon the NPX (see Fig. 7) where the hydrogens are located on the carbon atoms of the drug with the blue colors (belong to electron-poor areas), and the regions of a negative electrostatic potential

Table 2
Values of adsorption energy, nearest-neighbor distance, thermodynamic parameters and dipole moment of all the states in the water phase.

State	E_{sol}/kcal/mol	D/Å	μ_D/Debye
I	−28.59	1.532	10.31
II	−8.99	1.999	8.42
III	−8.30	2.889	8.26
IV	−9.45	2.177	8.12
G	−11.41	2.874	8.18
H	−9.81	3.317	4.77
OHB$_{12}$N$_{12}$	−59.49	1.341	2.23
X	−13.14	1.521	10.59
Y	−2.77	1.882	3.31

Table 3
Calculated HOMO energy (E_{HOMO}/eV), LUMO energy (E_{LUMO} /eV), Fermi level (E_F), energy gap (E_g/eV), and change of energy gap (ΔE_g/%) for $B_{12}N_{12}$ fullerene-like cage interacting with NPX in the gas and water phases.

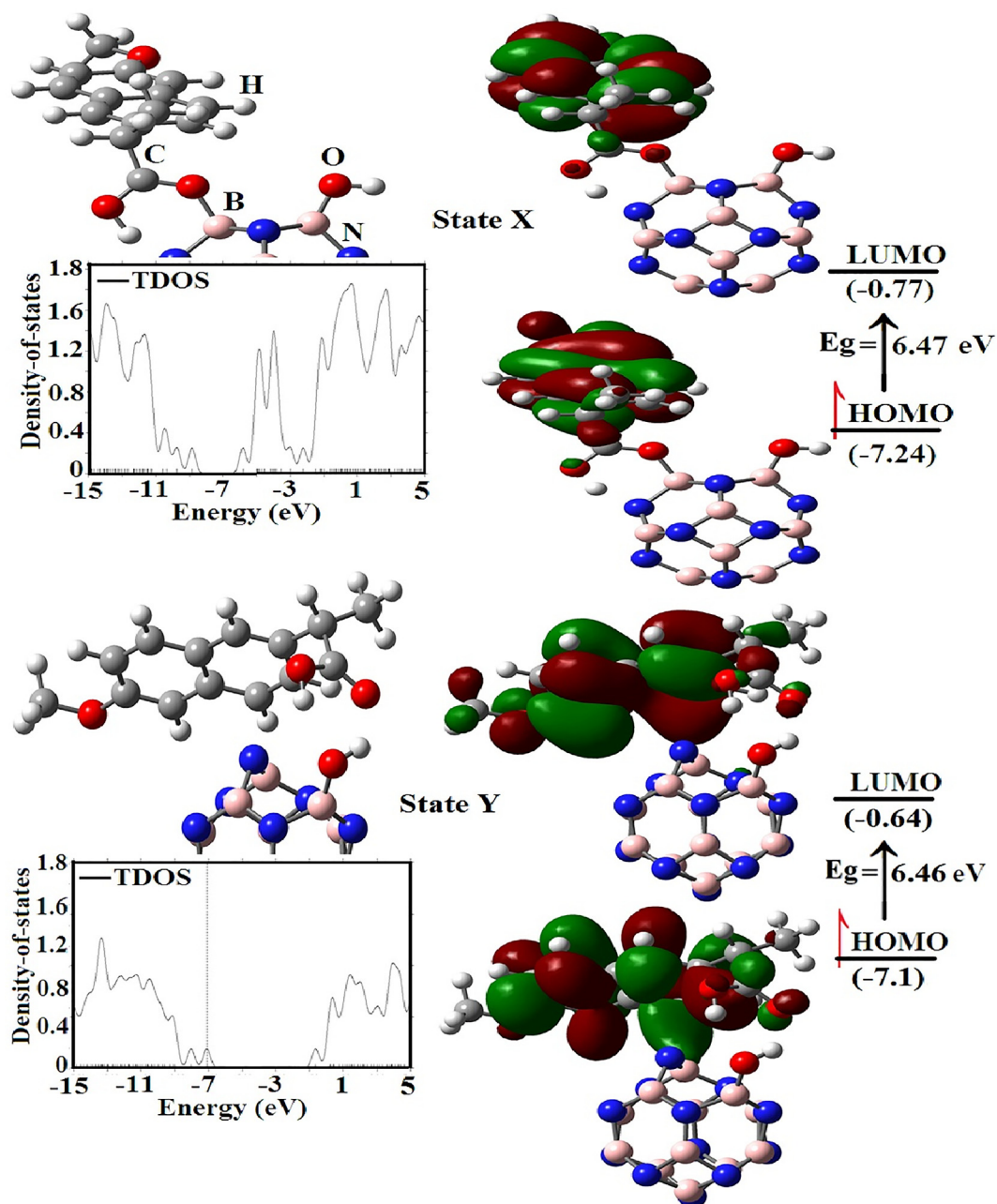| Property	E_{HOMO}/eV	E_{LUMO} /eV	E_g/eV	ΔE_g/%	E_F/eV
Gas					
NPX					
$B_{12}N_{12}$	−9.46	−0.01	9.51	–	−4.42
I	−7.28	−0.83	6.45	32.17	−4.76
II	−7.37	−0.85	6.52	31.44	−4.11
III	−7.29	−0.73	6.56	31.02	−4.11
IV	−7.38	−0.85	6.53	31.33	−4.76
Water					
NPX	−7.15	−0.6	6.55	–	−3.88
$B_{12}N_{12}$	−9.44	0.07	9.51	–	−4.69
I	−7.25	−0.79	6.46	32.07	−4.02
II	−7.22	−0.75	6.47	31.97	−3.99
III	−7.27	−0.73	6.54	31.23	−4.00
IV	−7.29	−0.73	6.56	31.02	−4.01

Fig. 6. HOMO-LUMO profiles of state X and state Y of NPX-OHB$_{12}$N$_{12}$ complex.

with the yellow–red colors happen on the B-N bonding [85]. The green color implies region with the neutral electrostatic potential. These plots represent that the charge transfer occurred from the drug (blue color) to the fullerene-like cage [86,87].

As illustrated in Fig. 8, the larger ELF value (Z≈ 1.0) placed on the B-N bonds exhibits a chemical covalent bond that may be formed through the NPX molecule adsorption on the B$_{12}$N$_{12}$ and OH-B$_{12}$N$_{12}$ fullerene-like cages [88]. In states I and X, ELF images implies the covalent interaction between both species with C—O···B bonds. Also, ELF images show the weak chemical interaction (unshared-electron interactions) on the species with intramolecular O—H···O hydrogen bonds between the NPX and the B$_{12}$N$_{12}$ in state Y suggesting a low sensitivity between them [89], therefore the release of the NPX molecule in such well-known OH-B$_{12}$N$_{12}$ is easier and could be too fast in contrary to the B$_{12}$N$_{12}$ and B$_{12}$P$_{12}$ fullerene-like cages.

3.7. Vibrational spectroscopy

We evaluated the infrared (IR) frequency and intensity of NPX before and after interact with B$_{12}$N$_{12}$ fullerene-like cage at the DFT level. The computed IR spectra of NPX and B$_{12}$N$_{12}$ complexes are depicted in Figs. 1 and 2. For the NPX drug, three bands at 1325, 1721, and 3342 cm^{-1} were assigned to the stretch of δCH$_3$, C=O, and O-H groups, respectively, which is close to mentioned results by other literatures [90]. In the IR spectra of the NPX [91], the observed bands at 3168, 3180, 3196 and 3215 cm^{-1} are attributed to C-H stretching vibration of aromatic hydrogen in NPX drug. The IR spectrum of the pure B$_{12}$N$_{12}$ fullerene-like was recorded in Fig. 2. The pure fullerene-like presents two distinct bands around 1441 and 816 cm^{-1}, which are the stretching vibrations of B-N bonds and the radial motion of the four squares [92,93]. After the IR spectra of the NPX adsorbed upon B$_{12}$N$_{12}$ fullerene, the calcu-

Table 4
Calculated HOMO energy (E_{HOMO}/eV), LUMO energy (E_{LUMO} /eV), Fermi level (E_F), energy gap (E_g, eV) for OH-$B_{12}N_{12}$ fullerene-like cage interacting with NPX in the gas and water phases.

Property	E_{HOMO}/eV	E_{LUMO} /eV	E_g/eV	ΔE_g/%	E_F/eV
Gas					
NPX	−6.98	−0.43	6.55	–	−3.71
OHB$_{12}$N$_{12}$	−9.18	0.03	9.21	3.15	−4.58
X	−7.24	−0.77	6.47	29.75	−4.00
Y	−7.1	−0.64	6.46	29.85	−3.87
Water					
NPX	−7.15	−0.6	6.55	–	−3.88
OHB$_{12}$N$_{12}$	−9.17	0.08	9.25	2.73	−4.55
X	−7.25	−0.81	6.44	30.37	−4.03
Y	−7.10	−0.64	6.46	30.16	−3.87
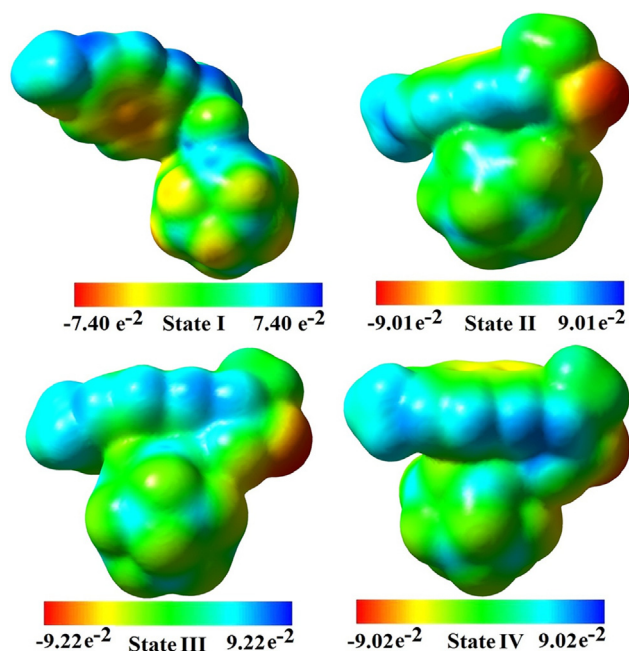
Fig. 7. MEP plots for NPX-$B_{12}N_{12}$ complexes in state I, II, III and IV.

lated υ(O—H), υ(C=O) and υ(C—O) stretching vibrations are significantly downshifted from 3371, 1728 and 1266 cm^{-1} to 3250, 1714, 1093 cm^{-1} at the state **I**, 3250, 1714, 1093 cm^{-1} at the state **II**, and 3611, 1881, 1091 cm^{-1} at the state **III** respectively, because of the attachment of the NPX molecule on the fullerene surface [94]. The calculated frequencies were scaled with scaling factor of 0.9854 for M06-2X functional. The calculated υ_{sy}(C—C) ring stretching vibrational modes of NPX interact with $B_{12}N_{12}$ fullerene appeared at 1646 cm^{-1} (**I**), 1642 cm^{-1} (**II**), and 1641 cm^{-1} (**III**) and in a free single NPX is appeared at 1610 cm^{-1}, and in the comparison with the experimental value 1603 cm^{-1}, as we see, the result at M06-2X functional is a relatively good match of the value [95]. The error between the theoretical and experimental values is 7 cm^{-1} for M06-2X functional. We observed in each three complexes, the C=C stretching vibrations in phenyl ring are appeared at 1537 and 1646 cm^{-1} in the state **I**, 1532 and 1642 cm^{-1} in the state **II**, and 1537 and 1646 cm^{-1} in the state **III**.

3.8. Assessment of optical properties

The ultraviolet–visible spectra (UV–Vis) of pure NPX, $B_{12}N_{12}$, and NPX-$B_{12}N_{12}$ complex were calculated by a time-dependent density functional theory (TDDFT) technique, as displayed in Table 5. The validity that the TDDFT/M06-2X functional is used to calculate excitation energy (E), oscillator strength (f), and the maximum excitation wavelength (λ_{max}), was described in references [11]. The bands of transitions in drug and fullerene-like cage will overlap when the spectra of a mixture comprising NPX and $B_{12}N_{12}$ is measured, even in the case that interaction happen. In UV–Vis absorption spectra, the first vertical S_1 (H → L + 1, %42) excitation of NPX drug takes place at 211 nm (5.86 eV) has the highest oscillator strength (f = 1.377) of the 30 highest transitions computed, followed by two bands at 221 nm (with an E of 6.47 eV and f of 0.2314) and 286 nm (with an E of 4.33 eV and f of 0.0637). Musa and Eriksson theoretically reported the main band of the naproxen at 217 nm with a remarkable oscillator strength 0.58 [96]. Perez *et al.* experimentally reported the UV–Vis spectra of NPX with the three bands calculated at 230 nm, 280 nm, and 320 nm [97]. Theoretical study exhibited that the computed results of M06-2X functional should be reliable for the assessment of optical properties. The $B_{12}N_{12}$ fullerene has a significant band with the λ_{max} of 205 nm and the E value of 6.05 eV close to the reported results by Soltani and Auyb [29,98]. Song *et al.* experimentally reported the absorption spectrum of boron nitride layers with one sharp absorption peak at 203 nm and showed a large optical energy band gap of 5.5 eV [99]. On the interaction between the NPX and the fullerene-like cage, the absorption wavelengths happen in the ultraviolet region, at the wavelength of 214 nm and f value of 0.6608 (A), 220 nm and f value of 0.6970 (B), 218 nm and f value of 0.7269 (C), and 221 nm and f value of 0.4545 (D), as displayed in Table 5.

3.9. Molecular docking studies of NPX loaded with $B_{12}N_{12}$ and OH-$B_{12}N_{12}$ nanocages

We have shown that NPX loaded with $B_{12}N_{12}$ and OH-$B_{12}N_{12}$ can preferentially inhibit pro-inflammatory cytokines such as tumour necrosis factor-alpha receptor and interleukin-1 receptor targets. To evaluate the inhibition mechanism of tumour necrosis factor-alpha receptor, the chosen complexes (NPX) were docked in the binding pocket of tumour necrosis factor-alpha receptor protein (PDB ID: 2AZ5). The best docking orientations of the NPX/OH-$B_{12}N_{12}$ with TNF-α and IL-1 have been presented in Figs. 9 and 10. It was found that complex consists of NPX loaded OH-$B_{12}N_{12}$ is potent inhibitors of TNF-α compared to NPX loaded $B_{12}N_{12}$ and $B_{12}P_{12}$ complexes. The calculated values of the binding pocket of TNF-α receptor protein for the $B_{12}N_{12}$, $B_{12}P_{12}$ and OH-$B_{12}N_{12}$ were found to be −7.7, −6.5, and −8.4 kcal/mol, respectively. Our calculated results presented that OH-$B_{12}N_{12}$ exerted a rapid anti-inflammatory effect on two proinflammatory cytokines, TNF-α and IL-1, compared to $B_{12}N_{12}$ and $B_{12}P_{12}$ systems. The calculated binding energies of the complexes showed that the binding pocket of TNF-α receptor protein for NPX loaded OH-$B_{12}N_{12}$ at the states X and Y were −10.6 and −10.5 kcal/mol, while the values of the binding pocket for NPX loaded $B_{12}P_{12}$ and $B_{12}N_{12}$ were −9.5 and −10.2 kcal/mol, respectively (Table 1). The NPX loaded OH-$B_{12}N_{12}$ is stabilized in the binding pocket of TNF-α receptor by polar interactions by several amino acid residues such as Tyr59, Tye151, Gly121 and Ser60 in chain B and also amino acids residues such as Gly121, Gln61, Gly122, His15, Tyr151, Tyr59, Tyr119, and Ser60 in chain A. Moreover, the NAP/OH-$B_{12}N_{12}$ complex was bounded with Leu120 in chain A and B via hydrophibic interactions. The results obtained revealed that the NAP/OH-$B_{12}N_{12}$ complex was bounded with key amino acid residues in the active site resulting in the inhibition of the TNF-α receptor [100,101] (Fig. 9). Furthermore, amino acid residues such as Tyr119 and Tyr151 interacted with the NAP/OH-$B_{12}N_{12}$ complex in the binding
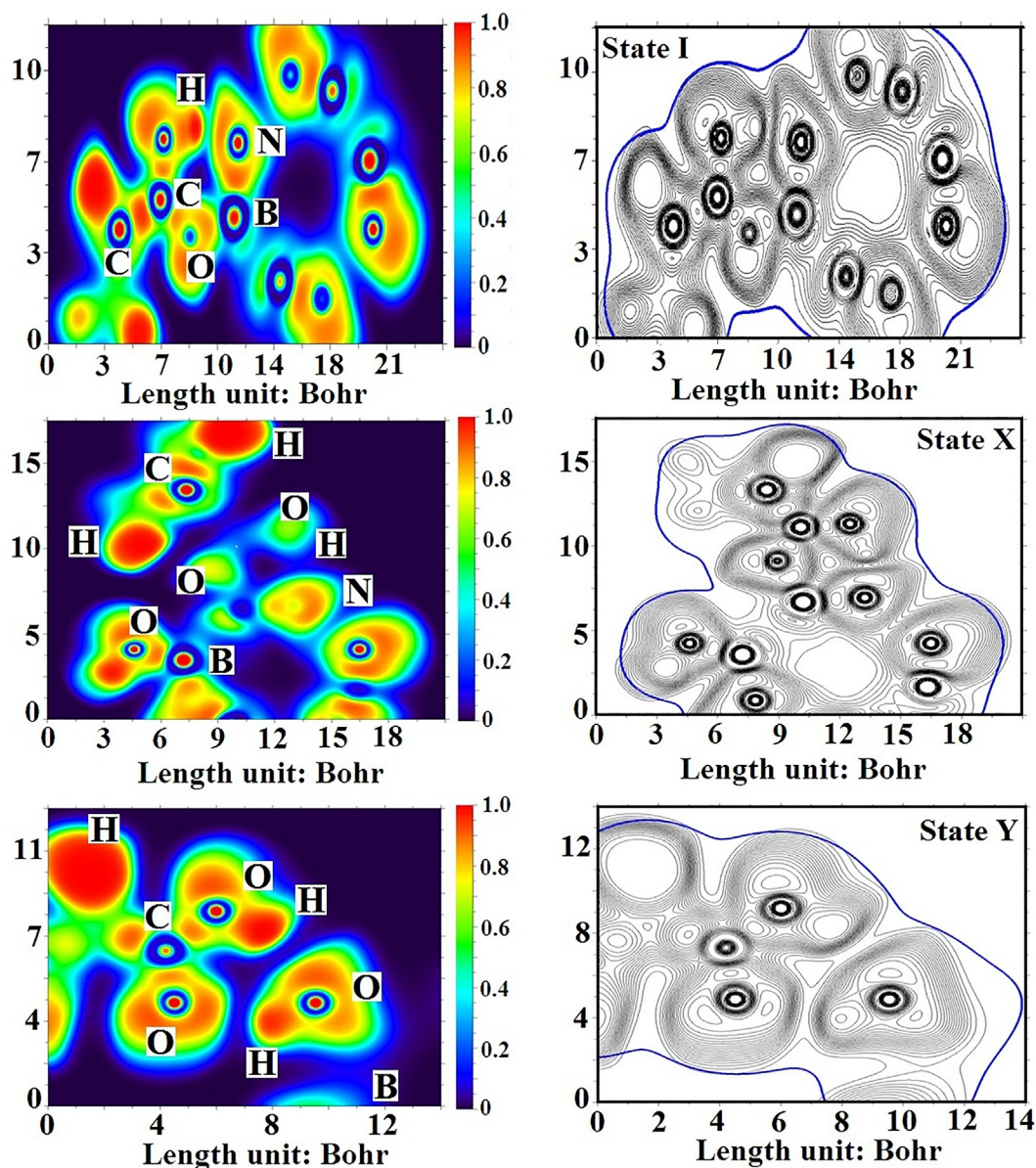
Fig. 8. Electron localized function (ELF) and contour line plots for NPX interacting with the $B_{12}N_{12}$ and OH-$B_{12}N_{12}$ fullerene-like cages.

pocket of the receptor by two hydrogen bonds which were 3.69 and 3.34 Å respectively.

The calculated binding energies of the complexes showed that the binding pocket of IL-1 receptor targets (PDB ID: 2L5X) for NPX loaded OH-$B_{12}N_{12}$ at the states X and Y was −10.5 and −10.4 kcal/mol, while the values of the binding pocket for NPX loaded $B_{12}P_{12}$ and $B_{12}N_{12}$ were −9.4 and −10.1 kcal/mol, respectively (Table 6). Furthermore, the naproxen complex was established in the binding pocket of the target via polar interactions by several amino acid residues such as Gln67, Lys61, Asp64, Tyr12, Thr103, Gly104, Ser105, Ser34, ASn9, Gln37, Asn36, Ser69, and Gln27. Moreover, amino acid residues such as Val35 and Met60 interacted via hydrophobic interactions. Furthermore, the NAP/OH-$B_{12}N_{12}$ complex is stabilized in the binding pocket of the receptor by four hydrogen bonds with the residues of protein such as Glu27, Gly104, Thr103 and Asn36. Hydrogen bond lengths were 3.60, 3.67, 3.90 and 3.39 Å respectively. 3D model for the binding mode showed that the NAP/OH-$B_{12}N_{12}$ complex was buried in

the pockets of the IL-1 receptor (Fig. 9). A comparison of molecular docking results demonstrated that the NAP/OH-$B_{12}N_{12}$ system had higher binding energy to the target structure with a strong interaction towards the binding pocket of the target, which more effectively inhibits the active site of the protein than the NAP/$B_{12}N_{12}$ and NAP/$B_{12}P_{12}$ systems. However, the hydrophobic and polar interactions might act a substantial role in occupation of the binding pocket. Our calculations showed that the NAP/OH-$B_{12}N_{12}$ complex could be a potential inhibitor of the TNF-α and IL-1 receptor at the binding site.

4. Conclusions

We evaluated the geometries, electronic, and optical features of the pure and OH-$B_{12}N_{12}$ fullerene-likes interacting with NPX drug through various functional groups (hydroxyl and carbonyl) in both in the vacuum and water environments. Our calculation represents

Table 5
Calculated optical spectra data of NPX adsorbed on the fullerene-like cages using TD-DFT/M06-2X/6-311G** functional.

| Methods	E/eV	λ_{max}/nm	f/a.u.	Assignment
NPX	5.86	211	1.3775	H-1 → L (40%), H → L + 1 (42%), H-3 → L + 2 (4%)
	6.47	221	0.2314	H-3 → L + 2 (21%), H-3 → L + 3 (15%), H-2 → L + 2 (8%)
	4.33	286	0.0637	H → L (78%), H-1 → L (7%), H → L + 1 (8%)
$B_{12}N_{12}$	6.05	205	0.001	H-1 → L + 1 (75%), H → L + 2 (12%)
	6.06	204	0.001	H-2 → L + 2 (42%), H → L + 2 (33%)
	6.07	204	0.001	H-2 → L + 1 (18%), H-2 → L + 3 (27%)
A	5.78	214	0.6608	H-1 → L (27%), H-1 → L + 1 (19%), H → L + 2 (49%)
	6.02	206	0.6408	H-1 → L + 1 (53%), H → L + 2 (13%), H → L + 7 (10%)
	5.31	233	0.4112	H-1 → L (27%), H → L + 1 (51%), H → L + 2 (11%)
B	5.62	220	0.6970	H → L + 7 (4%)
	5.85	211	0.2724	H-1 → L (10%), H → L + 2 (24%), H → L + 4 (26%), H → L + 7 (13%)
	5.93	209	0.1552	H → L + 2 (45%), H → L + 3 (24%), H → L + 4 (11%)
C	5.67	218	0.7269	H-1 → L (38%), H → L + 1 (48%)
	5.83	212	0.2887	H → L + 2 (20%), H → L + 3 (17%), H → L + 4 (19%), H → L + 7 (26%)
	6.05	204	0.1022	H-1 → L + 1 (60%)
D	5.59	221	0.4545	H-1 → L (28%), H → L + 2 (42%), H → L + 3 (20%)
	5.87	211	0.4376	H-1 → L (13%), H → L + 2 (-11%), H → L + 4 (55%)
	5.69	217	0.1281	H → L + 1 (15%), H → L + 2 (11%), H → L + 3 (48%)
$OHB_{12}N_{12}$	5.95	208	0.0116	H-8 → L (52%), H-9 → L (14%), H-7 → L (7%)
	5.47	226	0.0024	H-9 → L (25%), H-5 → L (19%), H-4 → L (19%)
	3.91	316	0.0010	H-6 → L (26%), H-1 → L (20%), H → L (10%)
X	5.32	233	0.4528	H → L + 1 (24%), H → L + 2 (26%), H-1 → L (15%)
	4.35	285	0.0814	H → L (33%), H → L + 1 (33%)
	1.99	623	0.0221	H-2 → L (79%), H-5 → L (10%)
Y	5.81	213	0.3846	H → L + 1 (12%), H → L + 2 (11%), H-1 → L (7%)
	5.70	222	0.6650	H-1 → L (16%), H-1 → L + 1 (16%), H → L + 1 (9%)
	4.28	289	0.0784	H → L (40%), H → L + 1 (40%), H-1 → L (3%)
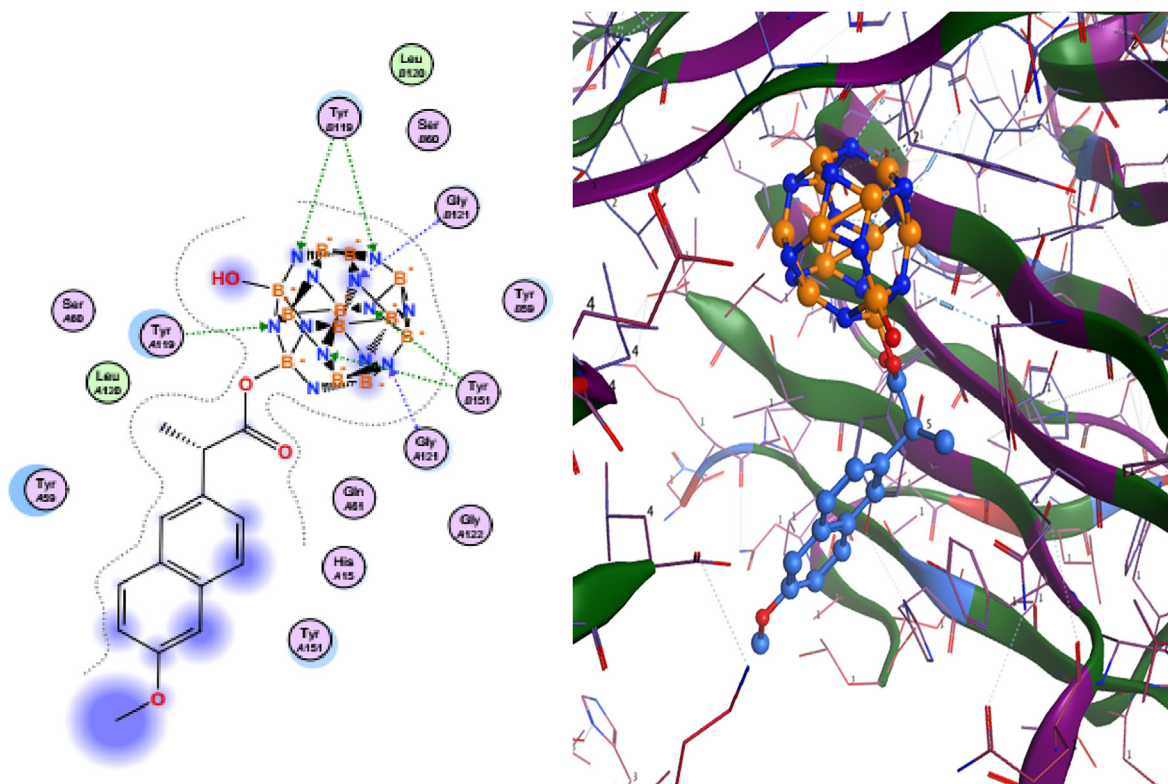
Fig. 9. Presentation of 2D and 3D models of interactions between NAP/OH-$B_{12}N_{12}$ complex and TNF receptor (PDB ID: 2AZ5).

that the functionalization of $B_{12}N_{12}$ and OH-$B_{12}N_{12}$ fullerene-likes (with the NPX drug from its carbonyl group than that of the hydroxyl group) exhibit significant thermodynamic stability. Then, we found that the adsorption of the NPX through the —C=O group over $B_{12}N_{12}$ fullerene-like is stronger than the —OH group in both environments. The increments of adsorption energy and charge
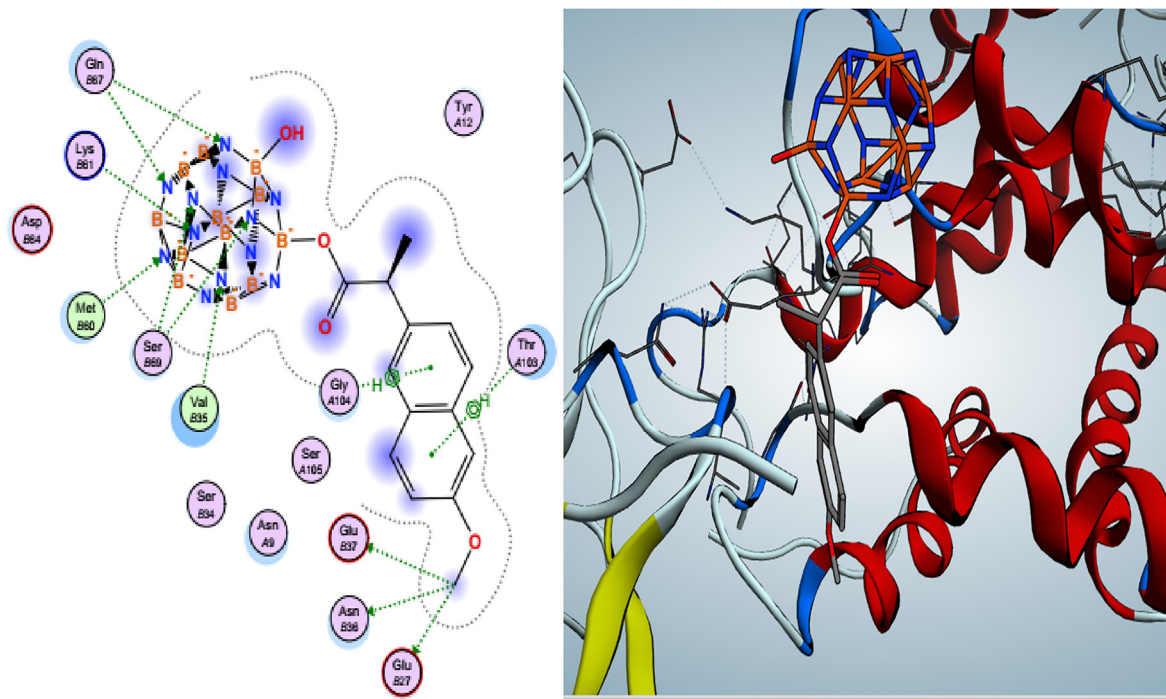
Fig. 10. Presentation of 2D and 3D models of interactions between NAP/OH-B$_{12}$N$_{12}$ complex and IL-1 receptor (PDB ID: 2LX5).

Table 6

Molecular docking simulations results for the complexes and TNF-α receptor (PDB ID: 2AZ5) , IL-1 receptor (PDB ID:2L5X).

Compound	PDB ID: 2AZ5		PDB ID:2L5X	
	Binding energy (kcal/mol)	inhibition constant(Ki) (μM)	Binding energy (kcal/mol)	inhibition constant(Ki) (μM)
NPX	−6.9	6.0	−6.7	6.1
B$_{12}$N$_{12}$	−7.7	5.4	−7.7	5.7
NPX-B$_{12}$N$_{12}$	−10.2	3.6	−10.1	3.8
B$_{12}$P$_{12}$	−6.5	6.1	−6.5	6.7
NPX-B$_{12}$P$_{12}$	−9.5	4.5	−9.4	4.7
OH-B$_{12}$N$_{12}$	−8.4	4.8	−8.4	5.2
State X	−10.6	3.1	−10.5	3.3
State Y	−10.5	3.5	−10.4	3.7

transfer exhibit that the states **I** and **X** could modify electronic and optical features of both fullerene-likes. A comparison between the theoretical frequencies and experimental results demonstrated an appreciable agreement with each other. The study of molecular docking exhibits the NAP/OH-B$_{12}$N$_{12}$ complex containing hydroxyl group has a good binding affinity with protein TNF-α and IL-1 in comparison with the other complexes. We hope that OH-B$_{12}$N$_{12}$ help for designing a novel drug carrier for the non-steroidal anti-inflammatory drugs.

CRediT authorship contribution statement

Yan Cao: Methodology, Writing - review & editing. **Afrasyab Khan:** Conceptualization, Formal analysis, Writing - original draft. **Fatemeh Ghorbani Analysis:** Writing - original draft. **Hassan Mirzaei:** Writing - review & editing. **Preeti Singla:** Writing - original draft, Data curation. **Hanzaleh Balakheyli:** Formal analysis, Writing - review & editing. **Alireza Soltani:** Supervision, Formal analysis, Writing - original draft. **Mehrdad Aghaei:** Formal analysis, Writing - review & editing. **Zivar Azmoodeh:** Formal analysis, Writing - review & editing. **Mehdi Aarabi:** Formal analysis, Writing - review & editing. **Samaneh Tavassoli:** Formal analysis, Writing - review & editing.

Declaration of Competing Interest

The authors declare that they have no known competing financial interests or personal relationships that could have appeared to influence the work reported in this paper.

Appendix A. Supplementary material

Supplementary data to this article can be found online at https://doi.org/10.1016/j.molliq.2021.116678.

References

[1] N. Okulik, A.H. Jubert, Theoretical study on the structure and reactive sites of three non-steroidal anti-inflammatory drugs: Ibuprofen, Naproxen and Tolmetin acids, J. Mol. Struct. (Thoechem) 769 (2006) 135–141.

[2] V. Erfani-Moghadam, M. Aghaei, A. Soltani, N. Abdolahi, A. Ravaghi, M. Cordani, S. Shirvani, S. Moazen Rad, H. Balakheyli, ST8 micellar/niosomal vesicular nanoformulation for delivery of naproxen in cancer cells: Physicochemical characterization and cytotoxicity evaluation, J. Mol. Struct. 1211 (2020) 127867.

[3] M.R. Rodrigues, C.M. Lanzarini, E. Ricci-Junior, Preparation, in vitro characterization and in vivo release of naproxen loaded in poly-caprolactone nanoparticles, Pharmaceut. Dev. Technol. 16 (2009) 12–21.

[4] S. Gianni Ciofani, G. Graziana Danti, D. D'Alessandro Genchi, J.-L. Pellequer, M. Odorico, V. Mattoli, M. Giorgi, Pilot in vivo toxicological investigation of boron nitride nanotubes, Int. J. Nanomed. 7 (2012) 19–24.

[5] G. Seifert, R.W. Fowler, D. Mitchell, D. Porezag, T. Frauenheim, Boron–nitrogen analogues of the fullerenes: electronic and structural properties, Chem. Phys. Lett. 268 (1997) 352–358.

[6] T. Oku, A. Nishiwaki, I. Narita, Formation and atomic structure of $B_{12}N_{12}$ nanocage clusters studied by mass spectrometry and cluster calculation, Sci. Technol. Adv. Mater. 5 (2004) 635–638.

[7] D. Golberg, Y. Bando, O. Stephan, K. Kurashima, Appl. Phys. Lett. 73 (1998) 2441–2443.

[8] T. Oku, M. Kuno, I. Narita, Diam. Relat. Mater. 11 (2002) 940.

[9] E. Shakerzadeh, E. Khodayar, S. Noorizadeh, Theoretical assessment of phosgene adsorption behavior onto pristine, Al- and Ga-doped $B_{12}N_{12}$ and $B_{16}N_{16}$ nanoclusters, Comput. Mater. Sci. 118 (2016) 155–171.

[10] E. Tazikeh-Lemeski, A. Soltani, M. Taghi Baei, M. Bezi Javan, S. Moazen Rad, Theoretical study on pure and doped $B_{12}N_{12}$ fullerenes as thiophene sensor, Adsorption 24 (2018) 585–593.

[11] A.S. Ghasemi, A. Soltani, M. Karimnia, F. Ashrafi, F. Heidari, M. Majidian, A study on the effect of 1-butyl-4-methylpyridiniumbromide adsorption on the structural and electronic properties of $B_{12}N_{12}$ nano-cage, J. Mol. Liq. 277 (2019) 115–122.

[12] E. Vessally, M.D. Esrafili, R. Nurazar, P. Nematollahi, A. Bekhradnia, A DFT study on electronic and optical properties of aspirin-functionalized $B_{12}N_{12}$ fullerene-like nanocluster, Struct. Chem. 28 (2017) 735–748.

[13] A. Soltani, A. Sousaraei, M. Bezi Javan, M. Eskandaric, H. Balakheyli, Electronic and optical properties of 5-AVAfunctionalized BN nanoclusters: a DFT study, New J. Chem. 40 (2016) 7018–7026.

[14] R. Guo, Q. Liu, W. Wang, R. Tayebee, F. Mollania, Boron nitride nanostructures as effective adsorbents for melphalan anti-ovarian cancer drug. Preliminary MTT assay and in vitro cellular toxicity, J. Mol. Liq. 325 (2021) 114798.

[15] N. Abdolahi, M. Aghaei, A. Soltani, Z. Azmoodeh, H. Balakheyli, F. Heidari, Adsorption of celecoxib on $B_{12}N_{12}$ fullerene: spectroscopic and DFT/TDDFT study, Spectrochim. Acta A 204 (2018) 348–353.

[16] A. Bahrami, S. Seidi, T. Baheri, M. Aghamohammadi, A first-principles study on the adsorption behavior of amphetamine on pristine, P- and Al-doped $B_{12}N_{12}$ nano-cages, Superlattices Microstruct. 64 (2013) 265–273.

[17] T. Oku, M. Kuno, H. Kitahara, I. Narita, Formation, atomic structures and properties of boron nitride and carbon nanocage fullerene materials, Int. J. Inorg. Mater. 3 (2001) 597–612.

[18] T. Oku, A. Nishiwaki, I. Narita, Sci. Technol. Adv. Mater. 5 (2004) 629.

[19] T. Oku, T. Hirano, M. Kuno, T. Kusunose, K. Niihara, K. Suganuma, Synthesis, atomic structures and properties of carbon and boron nitride fullerene materials, Mater. Sci. Eng., B 74 (2000) 206–217.

[20] A.S. Rad, K. Ayub, A comparative density functional Theory study of guanine chemisorption on $Al_{12}N_{12}$, $Al_{12}P_{12}$, $B_{12}N_{12}$, and $B_{12}P_{12}$ nano-cages, J. Alloy. Compd. 672 (2016) 161–169.

[21] A.S. Rad, Application of $B_{12}N_{12}$ and $B_{12}P_{12}$ as two fullerene-like semiconductors for adsorption of halomethane: study of density functional theory, Semiconductors 51 (2017) 134–138.

[22] Q. Weng, B. Wang, X. Wang, N. Hanagata, X. Li, D. Liu, X. Wang, X. Jiang, Y. Bando, D. Golberg, Highly Water-Soluble, Porous, and Biocompatible Boron Nitrides for Anticancer Drug Delivery, ACS, NANO 8 (2014) 6123–6130.

[23] M.A. Fernandez-Yague, A. Larrañaga, O. Gladkovskaya, A. Stanley, G. Tadayyon, Y. Guo, J.-R. Sarasua, S.A.M. Tofail, D.I. Zeugolis, A. Pandit, M.J. Biggs, Effects of Polydopamine Functionalization on Boron Nitride Nanotube Dispersion and Cytocompatibility, Bioconjug. Chem. 26 (10) (2015) 2025–2037.

[24] H. Zhang, T. Cheng, L. Lai, S. Deng, R. Yu, L. Qiu, J. Zhou, G. Lu, C. Zhi, J. Chen, BN nanospheres functionalized with mesoporous silica for enhancing CpG oligodeoxynucleotidemediated cancer immunotherapy, Nanoscale 10 (2018) 14516–14524.

[25] M.D. Esrafili, R. Nurazar, Methylamine adsorption and decomposition on $B_{12}N_{12}$ nanocage: A density functional theory study, Surf. Sci. 626 (2014) 44–48.

[26] X. Chen, J. Chang, H. Yan, D. Xia, Boron Nitride Nanocages as High Activity Electrocatalysts for Oxygen Reduction Reaction: Synergistic Catalysis by Dual Active Sites, J. Phys. Chem. C 120 (51) (2016) 28912–28916.

[27] A. Soltani, M.T. Baei, M. Ramezani Taghartapeh, E. Tazikeh Lemeski, S. Shojaee, Phenol interaction with different nano-cages with and without an electric field: a DFT study, Struct. Chem. 26 (2015) 685–693.

[28] M. Bezi Javan, A. Soltani, E. Tazikeh Lemeski, A. Ahmadi b, S. Moazen Rad, Interaction of B12N12 nano-cage with cysteine through various functionalities: A DFT study, Superlattic. Microstruct. 100 (2016) 24–37.

[29] A. Soltani, M. Ramezanitaghartapeh, M. Bezi Javan, M.T. Baei, A. Ng Kay Lup, P. J. Mahon, , Influence of the adsorption of toxic agents on the optical and electronic properties of $B_{12}N_{12}$ fullerene in the presence and absence of an external electric field, New J. Chem. 44 (2020) 14513–14528.

[30] Md. Rakib Hossain, Md. Mehade Hasan, M. Nishat, N-E. Ashrafi, F. Ahmed, T. Ferdous, Md. Abul Hossain, DFT and QTAIM investigations of the adsorption of chlormethine anticancer drug on the exteriorsurface of pristine and transition metal functionalized boron nitride fullerene, J. Mol. Liq. (2020) 114627.

[31] N. Abdolahi, P. Singla, A. Soltani, M. Javan, M. Aghaei, F. Heidari, S. Sedighi, Gold decorated $B_{12}N_{12}$ nanocluster as an effective sulfasalazine drug carrier: A theoretical investigation, Physica E 124 (2020) 114296.

[32] C.Y. Zhi, N. Hanagata, Y. Bando, D. Golberg, Dispersible Shortened Boron Nitride Nanotubes with Improved Molecule-Loading Capacity, Chem. Asian J. 6 (2011) 2530–2535.

[33] T. Sainsbury, A. Satti, P. May, Z. Wang, I. McGovern, Y.K. Gunko, J. Coleman, Oxygen Radical Functionalization of Boron Nitride Nanosheets, J. Am. Chem. Soc. 134 (2012) 18758–18771.

[34] C.Y. Zhi, Y. Bando, C.C. Tang, S. Honda, K. Sato, H. Kuwahara, D. Golberg, Covalent Functionalization: Towards Soluble Multiwalled Boron Nitride Nanotubes, Angew. Chem. Int. Ed. 44 (2005) 7932–7935.

[35] S.Y. Xie, W. Wang, K.A.S. Fernando, X. Wang, Y. Lin, Y.P. Sun, Solubilization of Boron Nitride Nanotubes, Chem. Commun. 29 (2005) 3670–3672.

[36] C.Y. Zhi, Y. Bando, C.C. Tang, R.G. Xie, T. Sekiguchi, D. Golberg, Perfectly Dissolved Boron Nitride Nanotubes Due to Polymer Wrapping, J. Am. Chem. Soc. 127 (2005) 15996–15997.

[37] Q. Huang, A.S.D. Sandanayaka, Y. Bando, C.Y. Zhi, R.Z. Ma, G.Z. Shen, D. Golberg, J.C. Zhao, Y. Araki, O. Ito, et al., Donor-Acceptor Nanoensembles Based on Boron Nitride Nanotubes, Adv. Mater. 19 (2007) 934–938.

[38] S. Pal, S.R.C. Vivekchand, A. Govindaraj, C.N.R. Rao, Functionalization and Solubilization of BN Nanotubes by Interaction with Lewis Bases, J. Mater. Chem. 17 (2007) 450–452.

[39] W.L. Wang, Y. Bando, C.Y. Zhi, W.Y. Fu, E.G. Wang, D. Golberg, Aqueous Noncovalent Functionalization and Controlled Near-Surface Carbon Doping of Multiwalled Boron Nitride Nanotubes, J. Am. Chem. Soc. 130 (2008) 8144–8145.

[40] A. Maguer, E. Leroy, L. Bresson, E. Doris, A. Loiseau, C.A. Mioskowski, Versatile Strategy for the Functionalization of Boron Nitride Nanotubes, J. Mater. Chem. 19 (2009) 1271–1275.

[41] Y. Lin, T.V. Williams, J.W. Connell, Soluble, Exfoliated Hexagonal Boron Nitride Nanosheets, J. Phys. Chem. Lett. 1 (2010) 277–283.

[42] Q. Weng, B. Wang, X. Wang, N. Hanagata, X. Li, D. Liu, X. Wang, X. Jiang, Y. Bando, D. Golberg, Highly Water-Soluble, Porous, and Biocompatible Boron Nitrides for Anticancer Drug Delivery, ACS Nano 8 (6) (2014) 6123–6130.

[43] Q. Weng, Q. Ide, X. Wang, X. Wang, C. Zhang, X. Jiang, Y. Xue, P. Dai, K. Komaguchi, Y. Bando, Design of Bn Porous Sheets with Richly Exposed (002) Plane Edges and Their Application as Tio$_2$ Visible Light Sensitizer, Nano Energy 16 (2015) 19–27.

[44] J. Grant, C. Carrero, F. Goeltl, J. Venegas, P. Mueller, S. Burt, S. Specht, W. McDermott, A. Chieregato, I. Hermans, Selective Oxidative Dehydrogenation of Propane to Propene Using Boron Nitride Catalysts, Science 354 (2016) 1570–1573.

[45] D. Farmanzadeh, M. Keyhanian, Computational assessment on the interaction of amantadine drug with $B_{12}N_{12}$ and $Zn_{12}O_{12}$ nanocages and improvement in adsorption behaviors by impurity Al doping, Theor. Chem. Acc. 138 (2019) 11.

[46] M. Bezi Javan, A. Soltani, Z. Azmoodeh, N. Abdolahi, N. Gholami, A DFT study on the interaction between 5-fluorouracil and $B_{12}N_{12}$ nanocluster, RSC Adv. 6 (2016) 104513–104521.

[47] A.S. Ghasemi, A. Ramezani Taghartapeh, A. Soltani, P.J. Mahon, Adsorption behavior of metformin drug on boron nitride fullerenes: Thermodynamics and DFT studies, J. Mol. Liq. 275 (2019) 955–967.

[48] S. Martínez Cairo, C. Salgado Legorreta, F. Martínez Zurita, Effect of naproxen on serum concentrations of IL-I, IL-6, and TNF in patients with osteoarthritis, Rev. Alerg. Mex. 48 (4) (2001) 119–122.

[49] V.A. Guilherme, L.N.M. Ribeiro, A.C.S. Alcântara, S.R. Castro, G.H. Rodrigues da Silva, C.G. da Silva, M.C. Breitkreitz, J. Clemente-Napimoga, C.G. Macedo, H.B. Abdalla, R. Bonfante, C.M.S. Cereda, E. de Paula, Improved efficacy of naproxen loaded NLC for temporomandibular joint administration, Sci. Rep. 9 (2019) 11160.

[50] L. Goerigk, S. Grimme, A thorough benchmark of density functional methods for general main group thermochemistry, kinetics, and noncovalent interactions, Phys. Chem. Chem. Phys. 13 (2011) 6670–6688.

[51] R. Padasha, M. Rabbani Esfahani, A. Shokuhi Rad, The computational quantum mechanical study of sulfamide drug adsorption onto X12Y12 fullerene-like nanocages: detailed DFT and QTAIM investigations, J. Biomol. Struct. Dynamics (2020) 1–11.

[52] A. Khalili, M.T. Baei, S.H. Hosseini Ghaboos, Improvement of Antioxidative Activity of Apigenin by $B_{12}N_{12}$ Nanocluster: Antioxidative Mechanism Analysis, ChemistrySelect 5 (2020) 1829–1836.

[53] E. Vessally, M.D. Esrafili, R. Nurazar, P. Nematollahi, A. Bekhradnia, Struct. Chem. 28 (2017) 735–748.

[54] A. Bahrami, S. Seidi, T. Baheri, M. Aghamohammadi, Superlattice. Microst. 64 (2013) 265–273.

[55] G. Scalmani, M.J. Frisch, J. Chem. Phys. 132 (2010) 114110.

[56] Gaussian 09, Revision D.01, M.J. Frisch, G.W. Trucks, H.B. Schlegel, G.E. Scuseria, M.A. Robb, J.R. Cheeseman, G. Scalmani, V. Barone, B. Mennucci, G.A. Petersson, H. Nakatsuji, M. Caricato, X. Li, H.P. Hratchian, A.F. Izmaylov, J. Bloino, G. Zheng, J.L. Sonnenberg, M. Hada, M. Ehara, K. Toyota, R. Fukuda, J. Hasegawa, M. Ishida, T. Nakajima, Y. Honda, O. Kitao, H. Nakai, T. Vreven, J.A. Montgomery Jr., J.E. Peralta, F. Ogliaro, M. Bearpark, J.J. Heyd, E. Brothers, K.N. Kudin, V.N. Staroverov, R. Kobayashi, J. Normand, K. Raghavachari, A. Rendell, J.C. Burant, S.S. Iyengar, J. Tomasi, M. Cossi, N. Rega, J.M. Millam, M. Klene, J.E. Knox, J.B. Cross, V. Bakken, C. Adamo, J. Jaramillo, R. Gomperts, R.E. Stratmann, O. Yazyev, A.J. Austin, R. Cammi, C. Pomelli, J.W. Ochterski, R.L. Martin, K. Morokuma, V.G. Zakrzewski, G.A. Voth, P. Salvador, J.J. Dannenberg, S. Dapprich, A.D. Daniels, O. Farkas, J.B. Foresman, J.V. Ortiz, J. Cioslowski, D.J. Fox, Gaussian, Inc., Wallingford CT, 2009.

[57] G.M. Morris, R. Huey, W. Lindstrom, M.F. Sanner, R.K. Belew, D.S. Goodsell, A.J. Olson, AutoDock4 and AutoDockTools4: Automated docking with selective receptor flexibility, J. Comput. Chem. 30 (16) (2009) 2785–2791.

[58] H. Mirzaei, M. Shokrzadeh, S. Emami, Synthesis, cytotoxic activity and docking study of two indole-chalcone derivatives, J. Mazandaran University of Med. Sci. 27 (154) (2017) 12–25.

[59] H. Mirzaei, M. Keighobadi, S. Emami, An overview of anticancer chalcones with apoptosis inducing activity, J. Mazandaran University of Med. Sci. 26 (146) (2017) 254–268.

[60] M. Reddy, M. Hussain, T.R. Rao, T. Kishna, V. Pavani, Formulation and evaluation of naproxen oral disintegrating tablets, Int J Pharm. Biol. Sci 2 (2012) 303–316.

[61] M.D. Esrafili, R. Nurazar, A density functional theory study on the adsorption and decomposition of methanol on B₁₂N₁₂ fullerene-like nanocage, Superlattices Microstruct. 67 (2014) 54–60.

[62] J.L. Li, T. He, G.W. Yang, An all-purpose building block: B₁₂N₁₂ fullerene, Nanoscale 4 (2012) 1665–1670.

[63] M. Kian, E. Tazikeh-Lemeski, B₁₂Y₁₂ (Y: N, P) fullerene-like cages for exemestane-delivery; molecular modeling investigation, J. Mol. Struct. 1217 (2020) 128455.

[64] H. Zhu, C. Zhao, Q. Cai, X. Fu, F. Rashid Sheykhahmad, Adsorption behavior of 5-aminosalicylic acid drug on the B₁₂N₁₂, AlB₁₁N₁₂ and GaB₁₁N₁₂ nanoclusters: A comparative DFT study, Inorg. Chem. Commun. 114 (2020) 107808.

[65] S. Onsoria, E. Alipour, A computational study on the cisplatin drug interaction with boronnitride nanocluster, J. Mol. Graph. Model. 79 (2018) 223–229.

[66] A. Soltani, M.T. Baei, M. Mirarab, M. Sheikhi, E. Tazikeh Lemeski, The electronic and structural properties of BN and BP nano-cages interacting with OCN: A DFT study, J. Phys. Chem. Solids 75 (2014) 1099–1105.

[67] S. Hussain, S.A. Shahid Chatha, A.I. Hussain, R. Hussain, M.Y. Mehboob, T. Gulzar, A. Mansha, N. Shahzad, K. Ayub, Designing Novel Zn-Decorated Inorganic B₁₂P₁₂ Nanoclusters with Promising Electronic Properties: A Step Forward toward Efficient CO2 Sensing Materials, ACS Omega 25 (2020) 15547–15556.

[68] A. Shokuhi Rad, K. Ayub, A comparative density functional Theory study of guanine chemisorption on Al₁₂N₁₂, Al₁₂P₁₂, B₁₂N₁₂, and B₁₂P₁₂ nano-cages, J. Alloy. Compd. 672 (2016) 161–169.

[69] Z.Y. Yang, Y.F. Li, Z. Zhou, Functionalization of BN nanotubes with free radicals: electroaffinity-independent configuration and band structure engineering, Frontiers of Physics in China. 4 (2009) 378–382.

[70] A. Mortazavifar, H. Raissi, A. Akbari, DFT and MD investigations on the functionalized boron nitride nanotube as an effective drug delivery carrier for Carmustine anticancer drug, J. Mol. Liq. 276 (2019) 577–587.

[71] C.Y. Zhi, Y. Bando, T. Terao, C.C. Tang, H. Kuwahara, D. Golberg, Chemically Activated Boron Nitride Nanotubes, Chem. Asian J. 4 (2009) 1536–1540.

[72] Q. Weng, X. Wang, X. Wang, Y. Bando, D. Golberg, Functionalized hexagonal boron nitride nanomaterials: emerging properties and applications, Chem. Soc. Rev. 45 (2016) 3989–4012.

[73] T.Y. Zakharian, A. Seryshev, B. Sitharaman, B.E. Gilbert, V. Knight, L.J. Wilson, A Fullerene−Paclitaxel Chemotherapeutic: Synthesis, Characterization, and Study of Biological Activity in Tissue Culture, J. Am. Chem. Soc. 127 (36) (2005) 12508–12509.

[74] P. Chaudhuri, A. Paraskar, S. Soni, R.A. Mashelkar, S. Sengupta, Fullerenol−Cytotoxic Conjugates for Cancer Chemotherapy, ACS Nano 3 (9) (2009) 2505–2514.

[75] F.-Y. Hsieh, A.V. Zhilenkov§, I.I. Voronov, E.A. Khakina§, D.V. Mischenko, P.A. Troshin, S.-h. Hsu, Water-Soluble Fullerene Derivatives as Brain Medicine: Surface Chemistry Determines If They Are Neuroprotective and Antitumor, ACS Appl. Mater. Interfaces 9 (13) (2017) 11482–11492.

[76] G. Scalmani, M.J. Frisch, Continuous surface charge polarizable continuum models of solvation, I. General formalism. J. Chem. Phys. 132 (2010) 114110.

[77] P. Singla, M. Riyaz, S. Singhala, N. Goel, Theoretical study of adsorption of amino acids on graphene and BN sheet in gas and aqueous phase with empirical DFT dispersion correction, Phys. Chem. Chem. Phys. 18 (2016) 5597–5604.

[78] A. Shokuhi Rad, K. Ayub, Enhancement in hydrogen molecule adsorption on B₁₂N₁₂ nano-cluster by decoration of nickel, Int. J. Hydrogen Energy 41 (2016) 22182–22191.

[79] K. Ayub, Transportation of hydrogen atom and molecule through X₁₂Y₁₂ nano-cages, Int. J. Hydrogen Energy 42 (2017) 11439–11451.

[80] H. Xu, X. Tu, G. Fan, Q. Wang, X. Wang, X. Chu, Adsorption properties study of boron nitride fullerene for the application as smart drug delivery agent of anti-cancer drug hydroxyurea by density functional theory, J. Molecular Liquids 318 (2020) 114315.

[81] Y. Guo, W. Guo, Hydroxylation of a metal-supported hexagonal boron nitride monolayer by oxygen induced water dissociation, Phys. Chem. Chem. Phys. 17 (2015) 16428–16433.

[82] P. Fallahi, H. Jouypazadeh, H. Farrokhpour, Theoretical studies on the potentials of some nanocages (Al12N12, Al12P12, B12N12, Be12O12, C12Si12, Mg12O12 and C24) on the detection and adsorption of Tabun molecule: DFT and TD-DFT study, J. Mol. Liq. 260 (2018) 138–148.

[83] K. Nejati, A. Hosseinian, E. Vessally, A. Bekhradnia, L. Edjlali, A comparative DFT study on the interaction of cathinone drug with BN nanotubes, nanocages, and nanosheets, Appl. Surf. Sci. 422 (2017) 763–768.

[84] J.C. Escobar, M.S. Villanueva, A.B. Hernández, D. Cortés-Arriagada, E.C. Anota, Interactions of B12N12 fullerenes on graphene and boron nitride nanosheets: A DFT study, J. Mol. Graph. Model. 86 (2019) 27–34.

[85] A. Shokuhi Rad, K. Ayub, Enhancement in hydrogen molecule adsorption on B12N12 nano-cluster by decoration of nickel, International, Journal of Hydrogen, Energy 41 (2016) 22182–22191.

[86] E. Chigo Anota, D. Cortes Arriagada, A. Bautista Hernández, M. Castro, In silico characterization of nitric oxide adsorption on a magnetic [B₂₄N₃₆ fullerene/ (TiO₂)₂] nanocomposite, Appl. Surf. Sci. 400 (2017) 283–292.

[87] A. Soltani, M. Bezi Javan, M.T. Baei, Z. Azmoodeh, Adsorption of chemical warfare agents over C₂₄ fullerene: Effects of decoration of cobalt, J. Alloy. Compd. 735 (2018) 2148–2161.

[88] R. Rahman, D. Mazumdar, Ab-Initio Adsorption Study of Chitosan on Functionalized Graphene: Critical Role of Van Der Waals Interactions, J. Nanosci. Nanotechnol. 12 (2012) 1–7.

[89] Y. Javadzadeh, F. Ahadi, S. Davarana, G. Mohammadi, A. Sabzevarid, K. Adibkia, Preparation and physicochemical characterization of naproxen–PLGA nanoparticles, Colloids Surf. B 81 (2010) 498–502.

[90] D. Mahendiran, R. Senthil Kumar, A. Kalilur Rahiman, Heteroleptic silver(I) complexes with 2,2′:6′,2″-terpyridines and naproxen: DNA interaction, EGFR/ VEGFR2 kinase, growth inhibition and cell cycle arrest studies, Mater. Sci. Eng., C 76 (2017) 601–615.

[91] A. Soltani, M. Ramezani Taghartapeh, V. Erfani-Moghadam, M. Bezi Javane, F. Heidari, M. Aghaei, P.J. Mahon, Serine adsorption through different functionalities on the B₁₂N₁₂ and Pt-B₁₂N₁₂ nanocages, Mater. Sci. Eng., C 92 (2018) 216–227.

[92] L. Feng, Y. Lu, J. Kong, Z. Su, Theoretical studies on the structure and properties of BN clusters (BN)ₙ and endohedral metallo-BN clusters M@(BN)ₙ, Comput. Theor. Chem. 964 (2011) 56–64.

[93] V. Georgiadou, G. Makris, D. Papagiannopoulou, G. Vourlias, C. Dendrinou-Samara, Octadecylamine Mediated Versatile Coating of CoFe₂O₄ NPs for the Sustained Release of Anti-inflammatory Drug Naproxen and in vivo Target Selectivity, ACS Appl. Mater. Interfaces 8 (14) (2016) 9345–9360.

[94] L. Liu, H. Gao, Quantum chemistry study of molecular structure and vibrational spectrum of naprox, Spectrochim. Acta Part A Mol. Biomol. Spectrosc. 86 (2012) 131–138.

[95] R.M. Silverstein, F.X. Webster, Spectrometric Identification of Organic Compounds, sixth Edi, Jon Willey Sons Inc., New York, 1963.

[96] Klefah A.K. Musa, Leif A. Eriksson, Theoretical Study of the Phototoxicity of Naproxen and the Active Form of Nabumetone, J. Phys. Chem. A 112 (2008) 10921–10930.

[97] M. Perez, R. Concu, M. Ornelas, M. Natalia, D.S. Cordeiro, M. Azenha, A. Fernando Silva, Measurement artifacts identified in the UV–vis spectroscopic study of adduct formation within the context of molecular imprinting of naproxen, Spectrochim. Acta Part A Mol. Biomol. Spectrosc. 153 (2016) 661–668.

[98] K. Auyb, Are phosphide nano-cages better than nitride nano-cages? A kinetic, thermodynamic and non-linear optical properties study of alkali metal encapsulated X₁₂Y₁₂ nano-cages, J. Mater. Chem. C 4 (2016) 10919–10934.

[99] L. Song, L. Ci, H. Lu, P.B. Sorokin, C. Jin, J. Ni, A.G. Kvashnin, D.G. Kvashnin, J. Lou, I. Yakobson, P.M. Ajayan, Large Scale Growth and Characterization of Atomic Hexagonal Boron Nitride Layers, Nano Lett. 108 (2010) 3209–3215.

[100] M. Aghaei, M. Ramezanitaghartapeh, M. Javan, M.S. Hoseininezhad-Namin, H. Mirzaei, A. Shokuhi Rad, A. Soltani, S. Sedighi, A. Ng Kay Lup, V. Khori, P.J. Mahon, F. Heidari, Investigations of adsorption behavior and anti-inflammatory activity of glycine functionalized Al₁₂N₁₂ and Al₁₂ON₁₁ fullerene-like cages, Spectrochim. Acta Part A Mol. Biomol. Spectrosc. 246 (2021) 119023.

[101] S. Xu, H. Peng, N. Wang, M. Zhao, Inhibition of TNF-α and IL-1 by compounds from selected plants for rheumatoid arthritis therapy: In vivo and in silico studies, Trop. J. Pharm. Res. 17 (2) (2018) 277–285.